A Theoretical Investigation of the Decarbonylation of Methoxy(siloxy)carbene

Paul G. Loncke and Gilles H. Peslherbe*

Centre for Research in Molecular Modeling and Department of Chemistry & Biochemistry, Concordia University, Montréal, Québec, Canada H4B 1R6

Received: September 25, 2003; In Final Form: February 13, 2004

The decarbonylation of methoxy(siloxy)carbene ($CH_3O\ddot{C}OSiH_3$) has been investigated by means of ab initio molecular orbital theory and hybrid density functional theory calculations, in conjunction with the quantum theory of atoms in molecules. Pathways involving intramolecular front-side nucleophilic attack by the methoxy oxygen at silicon and by the siloxy oxygen at the methyl carbon have been examined. The pathway involving intramolecular front-side nucleophilic attack by the methoxy oxygen at silicon has been found to be *concerted* (one step, no intermediates) and *synchronous* (bond formation and dissociation occur at the same rate). In contrast, although the pathway involving intramolecular front-side nucleophilic attack by the siloxy oxygen at the methyl carbon appears to be concerted, it is *asynchronous*, with transition-state features that resemble a tight ion-pair intermediate comprising a methyl cation and a siloxycarbonyl anion. Pathways for decarbonylation involving the intermediacy of methyl silyl formate, as well as radicals, have also been investigated. The most energetically viable pathway for decarbonylation appears to be that involving intramolecular front-side nucleophilic attack by the methoxy oxygen at silicon.

Introduction

Intramolecular rearrangements of dioxycarbenes are relatively rare. These carbenes preferentially undergo intermolecular reactions with species such as electron-deficient alkenes, alkynes, and alcohols.[1−3] In the absence of carbene scavengers, they tend to undergo dimerization rather than intramolecular rearrangements.[1,4,5] Of the few dioxycarbene rearrangements reported, most seem to occur via a fragmentation−recombination mechanism involving radicals. In the 1960s, Crawford and Raap proposed that diethoxycarbene rearrangements involve initial fragmentation to radicals, which subsequently combine to afford products.[6] More recently, Venneri and Warkentin found evidence indicating that 1,2-allyl migrations and [2,3]-sigmatropic rearrangements in methoxyallyloxycarbenes involve initial fragmentation to methoxycarbonyl and allylic radicals that subsequently collapse to form esters.[7] The latter findings are supported by ab initio and density functional theory (DFT) studies on hydroxycarbene[8] and hydroxyallyloxycarbene[9] rearrangements, which revealed that a fragmentation−recombination mechanism involving radicals is energetically viable. Merkley et al. also reported evidence indicating that rearrangements of p-substituted benzyloxymethoxycarbenes[10] and benzyloxybenzyloxycarbenes[11] occur via radicals.

Methoxytriphenylsiloxycarbene, **II**, generated by thermolysis of 2-methoxy-2-triphenylsiloxy-5,5-dimethyl-Δ^3-1,3,4-oxadiazoline, **I**, has been reported to undergo 1,2-triphenylsilyl migration and decarbonylation, affording methyl triphenylsilylformate, **III**, and methyl triphenylsilyl ether, **IV**, respectively (cf. Scheme 1).[12] However, there are questions regarding the mechanisms of these intramolecular carbene rearrangements. We recently carried out thorough theoretical investigations of the mechanisms for 1,2-silyl migration and 1,2-methyl migration in methoxy(siloxy)carbene ($CH_3O\ddot{C}OSiH_3$) as a model system for carbene **II**.[13,14] Our results suggest that 1,2-silyl migration

SCHEME 1

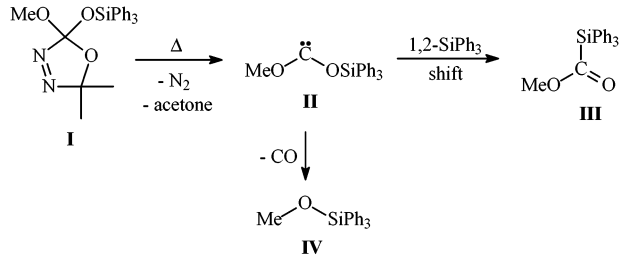

occurs via nucleophilic attack by the carbene lone pair at silicon, whereas 1,2-methyl migration appears to involve an anion-like shift of the methyl group from oxygen to the "vacant" carbene p orbital. We also found that 1,2-silyl migration is significantly more favorable than 1,2-methyl migration, in accord with experimental findings. We now turn our attention to the mechanism for decarbonylation of carbene **II**.

Decarbonylation of carbene **II** could occur via a fragmentation−recombination mechanism involving the intermediacy of carbon monoxide, along with either the methoxy and triphenylsilyl radicals or the methyl and triphenylsilyloxy radicals, similar to that proposed for decarbonylation of diethoxycarbene[6] and methoxycarbene.[15] However, since thermolysis of oxadiazoline **I** in toluene did not produce any bibenzyl and no products of radical trapping were detected in the presence of TEMPO (2,2,6,6-tetramethylpiperidinyloxy radical),[12] this mechanism seems unlikely, unless the radicals are formed within a solvent cage. Alternatively, decarbonylation could involve intramolecular front-side nucleophilic attack by either the methoxy oxygen at silicon or the siloxy oxygen at the methyl carbon. Moreover, this process could be concerted or stepwise, as discussed by Schreiner et al. for alkylchlorosulfite decomposition.[16,17]

The concerted mechanism for decarbonylation involving intramolecular front-side nucleophilic substitution would be a one-step process that occurs via a cyclic transition state as shown in Scheme 2a. However, it is evident from the frontier orbitals

* To whom correspondence may be addressed. E-mail: ghp@alcor.concordia.ca.

10.1021/jp036861m CCC: $27.50
Published on Web 06/25/2004

SCHEME 2

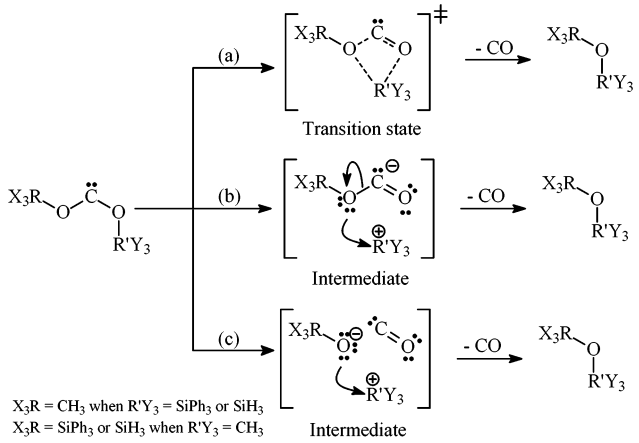

SCHEME 3

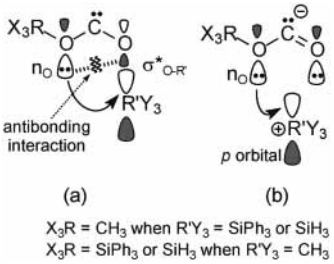

SCHEME 4

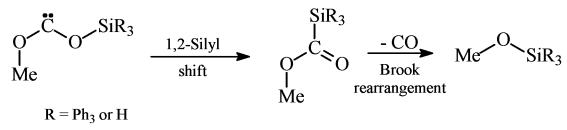

in Scheme 3a that this mechanism is *symmetry forbidden* according to Woodward−Hoffmann rules,[18−21] since interaction between the inplane "sp^2-hybridized" lone-pair n_O orbital (HOMO) and the $\sigma^*_{O-R'}$ antibonding orbital (LUMO) contains a destabilizing antibonding component. On the other hand, the stepwise mechanism would occur via an ion-pair intermediate. The ion-pair intermediate could consist of either a methoxycarbonyl anion and a triphenylsilyl cation or a triphenylsiloxycarbonyl anion and a methyl cation (cf. Scheme 2b).[22] Moreover, formation of such ion-pair intermediates would result in a *symmetry-allowed* reaction (cf. Scheme 3b), since it allows favorable bonding interaction between the in-plane "sp^2-hybridized" lone-pair n_O orbitals (HOMO) and the vacant cation p orbital (LUMO). Alternatively, the ion-pair intermediate could consist of carbon monoxide sandwiched between either a methoxide ion and a triphenylsilyl cation or a methyl cation and a triphenylsiloxide anion (cf. Scheme 2c), reminiscent of the tight ion-pair intermediates proposed by Moss et al. for the decarbonylation of alkoxyhalocarbenes.[23−32] However, the ion-pair mechanism is not likely to occur in a nonpolar solvent such as benzene.

Finally, in light of the fact that ester **III** undergoes decarbonylation when heated,[12,33,34] it is conceivable that decarbonylation of carbene **II** occurs via initial 1,2-triphenylsilyl migration to afford ester **III**, followed by a Brook rearrangement to yield ether **IV**, as outlined in Scheme 4. However, the rate constant for decarbonylation of ester **III** in benzene at 110 °C is 6.5×10^{-6} s^{-1}, which is smaller than the rate constant of 8.1×10^{-5} s^{-1} obtained for thermal decomposition of oxadiazoline **I** under similar conditions.[12] Thus, it seems that decarbonylation involving the intermediacy of ester **III** is unlikely. We note that when ester **III** was heated in methanol-d_4, a small amount of carbene **II** was trapped as the deuterated orthoformate $CH_3OCD(OCD_3)$-$OSiPh_3$, suggesting that decarbonylation of ester **III** could occur via carbene **II**. On the other hand, Brook et al. found evidence indicating that decarbonylation of ester **III** occurs via intramolecular front-side nucleophilic attack by the methoxy oxygen at silicon.[34]

In this article, we use ab initio molecular orbital theory and DFT calculations, along with the quantum theory of atoms in molecules, to investigate the decarbonylation of methoxy(siloxy)carbene as a model system for carbene **II**. Pathways involving intramolecular front-side nucleophilic attack by the methoxy oxygen at silicon and by the siloxy oxygen at the methyl carbon of the carbene are discussed. In addition, pathways involving the intermediacy of methyl silyl formate, as well as radicals [$H_3CO^\bullet$ + CO + $^\bullet SiH_3$] and [$H_3C^\bullet$ + CO + $^\bullet OSiH_3$], are examined.

Computational Methods

Ab initio molecular orbital calculations at the Hartree−Fock (HF) and second-order Møller−Plesset (MP2) levels of theory[35,36] and hybrid DFT calculations with the Becke3 Lee−Yang−Parr (B3LYP) hybrid functional[36,37] were performed with the 6-311+G(2d,p) basis set[35,36] using the Gaussian 98 suite of programs.[38] Calculations were carried out on the lowest singlet (S_0) state of methoxy(siloxy)carbene because of the large vertical $S_0 \rightarrow T_1$ energy gap.[13] Calculations involving radicals were performed with restricted open-shell HF and B3LYP and unrestricted MP2 methods, while calculations for all other species employed restricted methods. The 6-311+G(2d,p) basis was chosen after preliminary calculations with the 6-31+G(d), 6-311+G(2d,p), and 6-311++G(2df,pd) basis sets revealed that it yielded the best compromise between accuracy and performance. Geometry optimizations were performed using the default Berny algorithm[39] for minimum-energy structures and the eigenvector-following method[40−42] for transition-state structures. Frequency calculations were performed for stationary-point characterization and to obtain thermochemical data within the rigid rotor−harmonic oscillation approximation using standard statistical mechanics methods implemented in Gaussian 98.[43] Intrinsic reaction coordinate (IRC) calculations were used to connect transition states to reactants and products. The theory of atoms in molecules (AIM)[44] was used to analyze the electronic structure of the optimized geometries using the AIMPAC suite of programs.[44−46] Natural bond orbital (NBO) analysis[47] was carried out using the NBO program version 3.1 implemented in Gaussian 98.[48]

Results and Discussion

Ground-State Methoxy(siloxy)carbene Conformers. Minimum-energy geometries of the *trans-trans* **1**, *trans-cis* **2**, and *cis-trans* **3** conformers of methoxy(siloxy)carbene are shown in Figure 1. Optimized geometries of the transition states for trans-trans to trans-cis isomerization **TS$_{12}$** and trans-trans to cis-trans isomerization **TS$_{13}$** are also shown in the Figure 1. As suggested previously,[13] the electronic structure of the ground-state carbene conformers is most likely a hybrid of the three resonance structures shown in Scheme 5, where both the O2−C6 and C6−O7 bonds have partial double-bond character. Gradient vector analysis of the Laplacian of the electronic density,[49] $\nabla^2\rho(r)$, reveals that the valence-shell charge concentration (VSCC),[50] of the O2, C6, and O7 atoms each contain

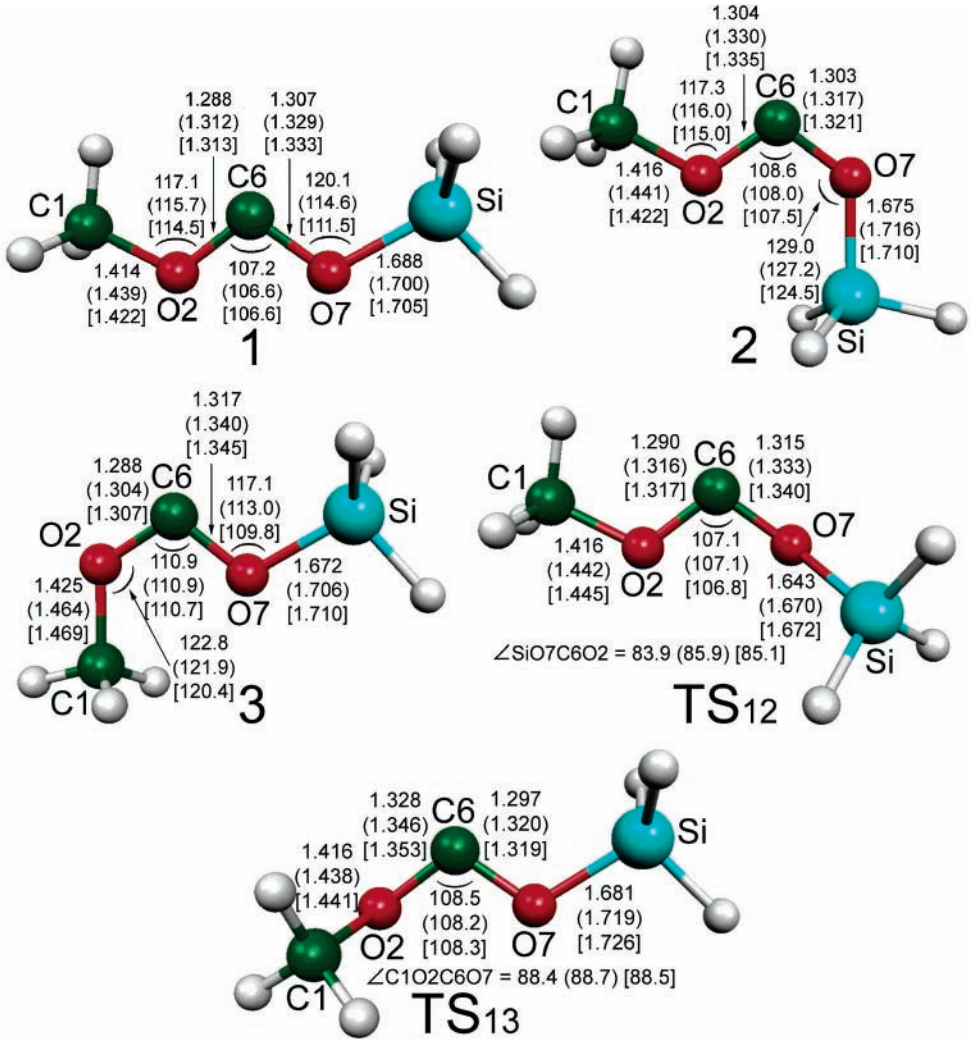

Figure 1. Optimized molecular geometries of the *trans-trans* **1**, *trans-cis* **2**, and *cis-trans* **3** conformers of methoxy(siloxy)carbene and the transition states for isomerization $\mathbf{TS_{12}}$ and $\mathbf{TS_{13}}$. Geometric parameters are given for the HF/6-311+G(2d,p), B3LYP/6-311+G(2d,p) (parentheses), and MP2/6-311+G(2d,p) [brackets] model chemistries. Bond distances and angles are in Å and degrees.

SCHEME 5

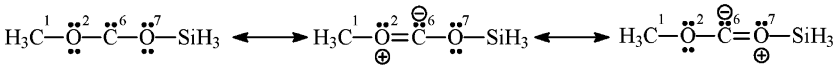

one nonbonded maximum. Since there is usually a one-to-one mapping between local maxima in the VSCC of an atom and electron pairs of the Lewis model,[44] these findings suggest that the O2, C6, and O7 atoms each possess a single lone pair. The second lone pair expected on the O2 and O7 atoms is apparently involved in π back-bonding with the vacant carbene p orbital, which gives rise to partial O2−C6 and C6−O7 double-bond character. In addition, it is evident from the topological properties of the electronic density $\rho(r)$ given in Table 1 that the bond critical point (BCP)[51] electronic density $\rho_b(r)$ for the O2−C6 and C6−O7 bonds are larger than that for the C1−O2 single bond. Moreover, values of the bond ellipticity,[52] ϵ, for the O2−C6 and C6−O7 bonds are noticeably larger than zero, consistent with the elliptical symmetry of the BCP electronic density usually associated with double bonds.[44] Hence, it is clear from these results that both the O2−C6 and C6−O7 bonds have considerable double-bond character. We note from the relative zero-point energy (ZPE) corrected electronic energies in Table 2 and Figure 2 that the computed barriers of trans-trans to cis-trans isomerization via $\mathbf{TS_{13}}$ are noticeably higher than those for trans-trans to trans-cis isomerization via $\mathbf{TS_{12}}$, indicating that the O2−C6 bond of conformer **1** has more double-bond character than the C6−O7 bond. This is supported by the fact that $\rho_b(r)$ for the O2−C6 bond of conformer **1** is larger than that for the C6−O7 bond (cf. Table 1).

Decarbonylation Involving Intramolecular Front-Side Nucleophilic Substitution. Let us now turn to methoxy(siloxy)-carbene decarbonylation involving intramolecular front-side nucleophilic attack by the methoxy oxygen at silicon and by the siloxy oxygen at the methyl carbon. It is evident from the frontier orbitals of conformer **1** shown in Figure 3 that the HOMO has considerable nonbonding character corresponding to inplane "sp^2-hybridized" lone-pair orbitals on the O2, C6, and O7 atoms (hereafter referred to as n_{O2}, n_{C6}, and n_{O7}), while the LUMO is essentially the σ^*_{O7-Si} antibonding orbital. The computed HF/6-311+G(2d,p) HOMO/LUMO gaps of conformers **1**, **2**, and **3** are 11.9, 11.8, and 11.8 eV, respectively. These gaps seem appropriate for intramolecular reactivity when compared to the HF/4-31G HOMO/LUMO gap of 11.7 eV for phenylacetoxycarbene,[53] which is known to undergo 1,2-acyl migration. In contrast, the HF/6-31G* HOMO/LUMO gap of dimethoxycarbene is 14.9 eV,[1] while the HF/4-31G HOMO/

TABLE 1: Topological Properties of the Electronic Density at Selected Bond Critical Points Obtained from AIM Analysis of B3LYP/6-311+G(2d,p) Wave Functions[a]

	C1−O2	O2−C6	C6−O7	O7−Si
		1		
$\rho_b(r)$ (e/Å^3)	1.62	2.19	2.11	0.84
$\nabla^2\rho_b(r)$ (e/Å^5)	−12.3	−13.2	−15.5	14.6
ϵ	0.01	0.13	0.17	0.05
		2		
$\rho_b(r)$ (e/Å^3)	1.61	2.09	2.14	0.80
$\nabla^2\rho_b(r)$ (e/Å^5)	−12.0	−13.3	−13.9	13.2
ϵ	0.00	0.16	0.16	0.02
		3		
$\rho_b(r)$ (e/Å^3)	1.55	2.22	2.05	0.83
$\nabla^2\rho_b(r)$ (e/Å^5)	−11.9	−12.5	−15.0	14.3
ϵ	0.00	0.11	0.20	0.05

TS_{26}

	C1−O2	O2−C6	C6−O7	O7−Si	O2−Si
$\rho_b(r)$ (e/Å^3)	1.53	1.48	2.62	0.48	0.41
$\nabla^2\rho_b(r)$ (e/Å^5)	−10.8	−10.2	−15.5	4.0	3.6
ϵ	0.01	0.27	0.01	0.13	0.47

TS_{36}

	C1−O2	O2−C6	C6−O7	O7−Si	C1−O7
$\rho_b(r)$ (e/Å^3)	0.19	2.91	1.90	0.79	0.28
$\nabla^2\rho_b(r)$ (e/Å^5)	1.7	−7.3	−12.8	13.1	2.4
ϵ	0.13	0.00	0.26	0.06	0.12

TS_{14}

	C1−O2	O2−C6	C6−O7	O7−Si	C6−Si
$\rho_b(r)$ (e/Å^3)	1.59	2.21	2.48	0.52	0.52
$\nabla^2\rho_b(r)$ (e/Å^5)	−11.7	−13.2	−17.3	6.8	4.1
ϵ	0.01	0.08	0.03	1.34	0.85

TS_{35}

	C1−O2	O2−C6	C6−O7	O7−Si	C6−Si
$\rho_b(r)$ (e/Å^3)	1.53	2.25	2.41	0.52	0.52
$\nabla^2\rho_b(r)$ (e/Å^5)	−11.4	−13.0	−16.8	6.9	4.2
ϵ	0.01	0.08	0.06	1.08	0.85

5

	C1−O2	O2−C6	C6−O7	C6−Si
$\rho_b(r)$ (e/Å^3)	1.60	2.04	2.87	0.77
$\nabla^2\rho_b(r)$ (e/Å^5)	−12.4	−17.1	−12.7	2.1
ϵ	0.00	0.00	0.09	0.08

TS_{56}

	C1−O2	O2−C6	C6−O7	C6−Si	O2−Si
$\rho_b(r)$ (e/Å^3)	1.68	0.82	3.21	0.44	0.56
$\nabla^2\rho_b(r)$ (e/Å^5)	−13.9	4.5	0.1	4.7	3.8
ϵ	0.01	0.24	0.04	0.59	0.18

[a] HF/6-311+G(2d,p) and MP2/6-311+G(2d,p) values are provided in the Supporting Information section.

LUMO gap of methoxyphenoxycarbene is 14.1 eV.[2] The latter two dioxycarbenes are not known for their intramolecular reactivity, which may be due in part to their larger HOMO/LUMO gaps. Thus, since the n_{O2} portion of the HOMO is aligned with the σ^*_{O7-Si} portion of the LUMO in conformer **2**, HOMO/LUMO interaction and hence nucleophilic attack by the methoxy oxygen O2 at silicon is expected to be favorable. In contrast, although the n_{O7} part of the HOMO would be aligned with the σ^*_{C1-O2} portion of the LUMO in conformer **3**, HOMO/LUMO interaction and thus nucleophilic attack by the siloxy oxygen O7 at the methyl carbon C1 is not expected to be favorable due to the lack of σ^*_{C1-O2} character of the LUMO (cf. Figure 3).

TABLE 2: Calculated Zero-Point Energy Corrected Electronic Energies of Species Involved in the Decarbonylation of Methoxy(siloxy)carbene[a]

species	B3LYP/6-311+G(2d,p)	MP2/6-311+G(2d,p)
1	0.0	0.0
2	2.0	2.3
3	1.9	1.6
TS_{12}	7.2	8.3
TS_{13}	17.5	18.3
TS_{26}	19.9	18.0
TS_{36}	40.2	-
TS_{14}	10.3	8.8
TS_{35}	9.5	7.8
4	−15.9	−17.4
5	−23.1	−24.7
TS_{45}	−10.4	−11.8
TS_{56}	9.9	5.0
$CH_3O^\bullet + CO + {}^\bullet SiH_3$	66.7	73.0
$CH_3^\bullet + CO + {}^\bullet OSiH_3$	53.0	56.9
6 + CO	−32.6	−39.1

[a] Relative energies with respect to conformer **1** are in kcal/mol. The total B3LYP/6-311+G(2d,p) and MP2/6-311+G(2d,p) energies for conformer **1** are −519.751601 and −518.678680 hartrees, respectively. Radicals were calculated using the ROB3LYP/6-311+G(2d,p) and UMP2/6-311+G(2d,p) methods. Calculated HF/6-311+G(2d,p) ZPE-corrected electronic energies are provided in the Supporting Information section.

The optimized transition-state geometries for methoxy(siloxy)carbene decarbonylation involving intramolecular front-side nucleophilic attack by the methoxy oxygen O2 at silicon in conformer **2** (denoted **TS_{26}**) and by the siloxy oxygen O7 at the methyl carbon C1 in conformer **3** (denoted **TS_{36}**) are shown in Figure 4. Optimized molecular geometries for the products, carbon monoxide and methyl silyl ether **6**, are also shown in Figure 4. IRC calculations confirm that **TS_{26}** and **TS_{36}** connect conformers **2** and **3**, respectively, to carbon monoxide and methyl silyl ether **6**. Thus, both reactions occur via concerted pathways instead of stepwise pathways involving tight ion-pair intermediates similar to those discussed earlier. Interestingly, although we were able to obtain the transition state **TS_{36}** at the HF and B3LYP levels with the 6-311+G(2d,p) basis set, and even at the MP2 level with smaller basis sets, we were unable to locate this transition state on the MP2/6-311+G(2d,p) potential energy surface.

Let us first examine the changes in geometry and electronic structure for methoxy(siloxy)carbene decarbonylation involving intramolecular front-side nucleophilic attack by the methoxy oxygen O2 at silicon. Relative to conformer **2** (cf. Figure 1), there is considerable shrinkage of the ∠C6O7Si angle, accompanied by modest O2−C6 and O7−Si bond lengthening and C6−O7 bond shortening, in **TS_{26}** (cf. Figure 4). These features are consistent with nucleophilic attack by the methoxy oxygen O2 at silicon, in concert with modest O2−C6 and O7−Si bond dissociation and C6−O7 triple-bond formation. Figure 5a displays plots of bond distances vs IRC for decarbonylation of conformer **2** via **TS_{26}**. Negative and positive IRC values correspond to the reactant and product sides of the reaction coordinate, respectively, while an IRC value of zero represents the transition state. The plots in Figure 5a clearly show that there is moderate O2−C6 and O7−Si bond lengthening and C6−O7 bond shortening, in going from conformer **2** to **TS_{26}**. More importantly, they illustrate that the reaction is *synchronous* in that the rates of O2−C6 and O7−Si bond lengthening and C6−O7 bond shortening are essentially identical as decarbonylation of conformer **2** approaches **TS_{26}**.

The shrinkage of the ∠C6O7Si angle in going from conformer **2** (cf. Figure 1) to **TS_{26}** (cf. Figure 4), which consequently

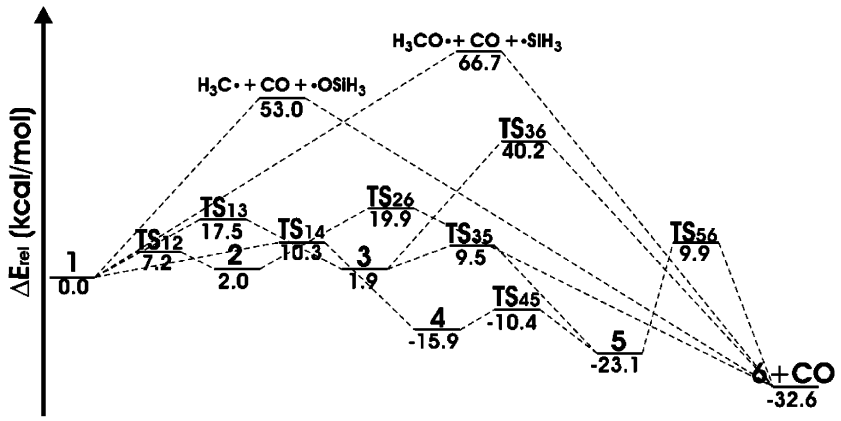

Figure 2. Relative B3LYP/6-311+G(2d,p) ZPE-corrected electronic energy profile of the methoxy(siloxy)carbene decarbonylation pathways.

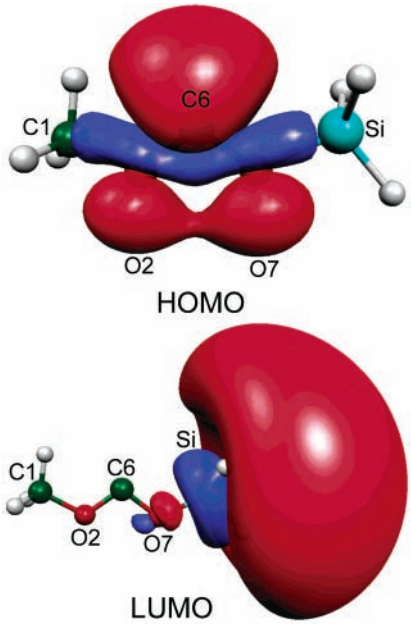

Figure 3. Plots of the computed HF/6-311+G(2d,p) frontier molecular orbitals for conformers **1** of methoxy(siloxy)carbene.

reduces the distance between the O2 and Si atoms, results in a new O2−Si bond with low $\rho_b(r)$ and positive $\nabla^2\rho_b(r)$ (cf. Table 1).[54] In addition, $\rho_b(r)$ for the lengthening O2−C6 and O7−Si bonds decreases while that for the shortening C6−O7 bond increases. These features are also consistent with nucleophilic attack by the methoxy oxygen O2 at silicon, along with O2−C6 and O7−Si bond dissociation and C6−O7 triple-bond formation. From the plots of BCP electronic densities vs IRC shown in Figure 5b, the decrease in $\rho_b(r)$ for the O2−C6 and O7−Si bonds and the increase in $\rho_b(r)$ for the C6−O7 bond are moderate and occur essentially at the same rate as the reaction proceeds from conformer **2** toward **TS$_{26}$**, further revealing the synchronicity of the reaction.

The synchronous nature of this *symmetry-forbidden* concerted reaction is most likely due to the fact that the destabilizing antibonding component of the $n_{O2} \rightarrow \sigma^*_{O7-Si}$ HOMO/LUMO interaction (cf. Scheme 3a) for nucleophilic attack by the methoxy oxygen O2 at silicon is small. NBO analysis[47] of the HF/6-311+G(2d,p) wave function for conformer **2** reveals that the polarization coefficients of the σ^*_{O7-Si} orbital are 14% on O7 and 86% on Si, which means that the σ^*_{O7-Si} orbital is primarily localized on the more electropositive Si atom. In other words, the σ^*_{O7-Si} orbital lobes are considerably smaller on O7 than they are on Si (cf. Scheme 3a). Therefore, only modest O2−C6 and O7−Si bond dissociation is needed to overcome the small destabilizing antibonding component of the $n_{O2} \rightarrow \sigma^*_{O7-Si}$ HOMO/LUMO interaction between lobes of opposite sign, while simultaneously allowing favorable bonding interaction between lobes of the same sign. We note that the synchronicity of this reaction is reminiscent of the concerted S_Ni (substitution nucleophilic internal) mechanisms proposed by Sommer et al. for organosilicon reactions involving three and four center cyclic transition states.[55−57]

We now consider the changes in geometry and electronic structure for methoxy(siloxy)carbene decarbonylation involving intramolecular front-side nucleophilic attack by the siloxy oxygen O7 at the methyl carbon C1. Relative to conformer **3** (cf. Figure 1), the ∠C1O2C6 angle shrinks significantly, while there is tremendous C1−O2 bond elongation, modest O2−C6 bond shortening, and slight C6−O7 bond lengthening in **TS$_{36}$** (cf. Figure 4). The latter features are also reflected in the plots of bond distances vs IRC shown in Figure 6a. These observations are consistent with nucleophilic attack by the siloxy oxygen O7 at the methyl carbon C1, in concert with tremendous C1−O2 bond dissociation, modest O2−C6 triple-bond formation, and slight C6−O7 bond dissociation. Moreover, the plots in Figure 6a show that the reaction is *asynchronous* in that the rate of C1−O2 bond elongation is considerably greater than the rates of O2−C6 bond shortening and C6−O7 bond lengthening. As a matter of fact, the geometry of **TS$_{36}$** resembles a tight ion-pair intermediate comprising a methyl cation and a siloxycarbonyl anion (cf. Scheme 2b). The computed HF/6-311+G(2d,p) and B3LYP/6-311+G(2d,p) ∠HC1H angles of **TS$_{36}$** are 117.8 and 118.3°, respectively, close to the 120° angle expected for a methyl cation.

The shrinkage of the ∠C1O2C6 angle in **TS$_{36}$** (cf. Figure 4) relative to conformer **3** (cf. Figure 1), which brings the C1 and O7 atoms in closer proximity to each other, yields a new C1−O7 bond with low $\rho_b(r)$ and positive $\nabla^2\rho_b(r)$ (cf Table 1). Simultaneously, $\rho_b(r)$ decreases dramatically for the lengthening C1−O2 bond, while it increases and decreases slightly for the shortening O2−C6 bond and lengthening C6−O7 bond, respectively. The latter observations are also evident from plots of the BCP electronic densities vs IRC for decarbonylation of conformer **3** via **TS$_{36}$** shown in Figure 6b. These findings are also in accord with front-side nucleophilic attack by the siloxy oxygen O7 at the methyl carbon C1, along with tremendous C1−O2 bond dissociation, moderate O2−C6 triple-bond formation, and slight C6−O7 bond dissociation. In addition, the plots in Figure 6b show that the rate of decrease in $\rho_b(r)$ for the C1−O2 bond is substantially larger than the rate of increase in $\rho_b(r)$ for the O2−C6 bond and the rate of decrease in $\rho_b(r)$ for the

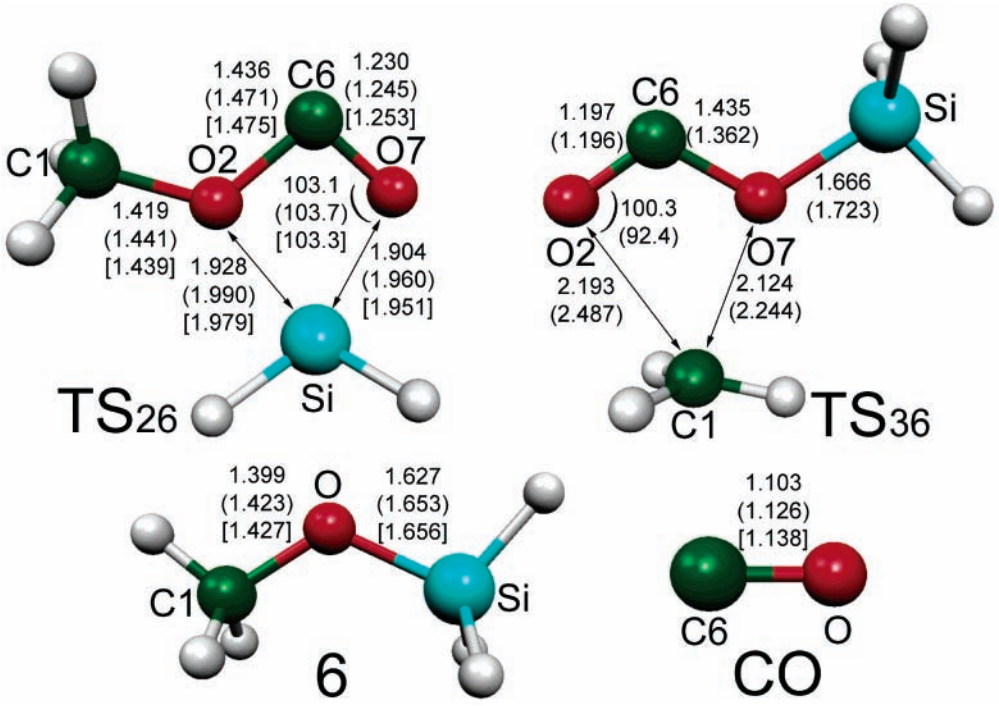

Figure 4. Optimized molecular geometries for **TS$_{26}$**, **TS$_{36}$**, **6**, and CO. Geometric parameters are given for the HF/6-311+G(2d,p), B3LYP/6-311+G(2d,p) (parentheses), and MP2/6-311+G(2d,p) [brackets] model chemistries. Bond lengths and angles are given in Å and degrees.

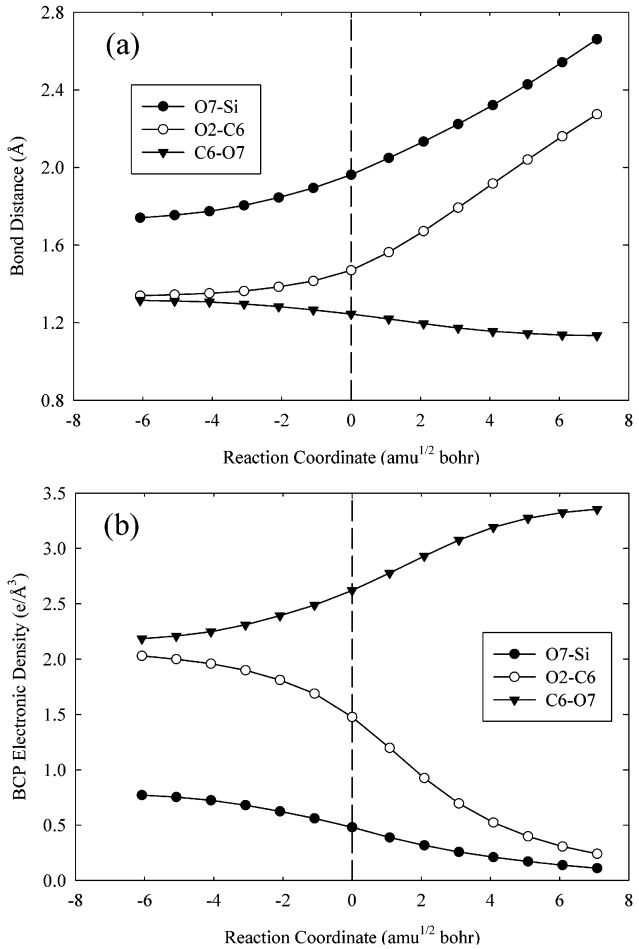

Figure 5. Plots of (a) bond distances vs IRC and (b) BCP electronic density vs IRC for decarbonylation of conformer **2** via **TS$_{26}$** based on B3LYP/6-311+G(2d,p) calculations.

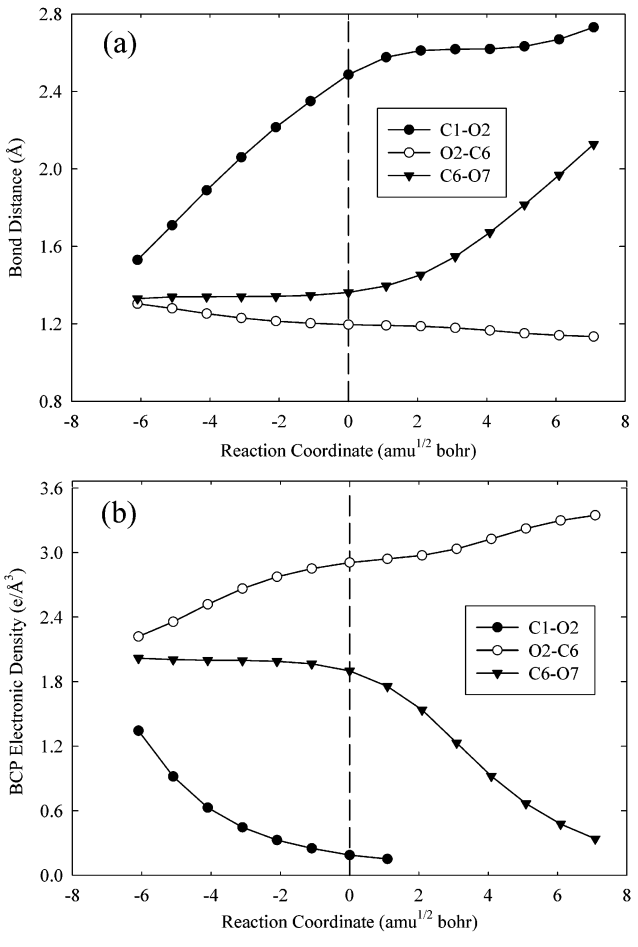

Figure 6. Plots of (a) bond distance vs reaction coordinate and (b) BCP electronic density vs reaction coordinate for decarbonylation of conformer **3** via **TS$_{36}$** based on B3LYP/6-311+G(2d,p) calculations.

C6−O7 bond as decarbonylation of conformer **3** approaches **TS$_{36}$**, further revealing the asynchronous nature of the reaction.

The asynchronous nature of this *symmetry-forbidden* concerted reaction is most likely due to the fairly sizable destabiliz-

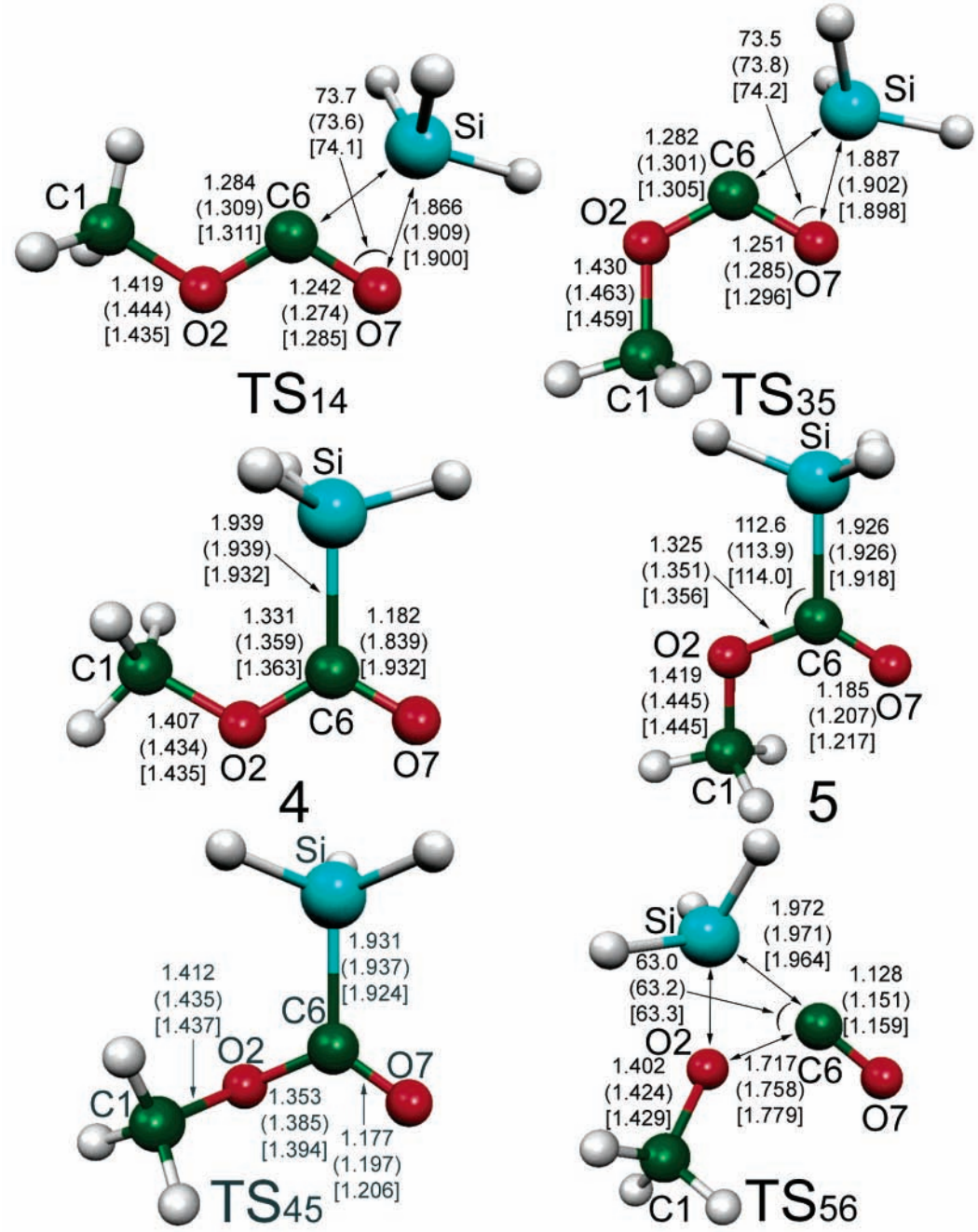

Figure 7. Optimized molecular geometries for **TS$_{14}$**, **TS$_{35}$**, **4**, **5**, **TS$_{45}$**, and **TS$_{56}$**. Geometric parameters are given for the HF/6-311+G(2d,p), B3LYP/6-311+G(2d,p) (parentheses), and MP2/6-311+G(2d,p) [square brackets] model chemistries. Bond lengths and angles are in Å and degrees.

SCHEME 6

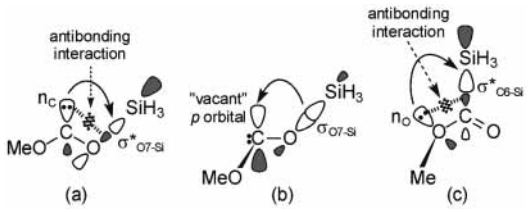

ing antibonding component of the $n_{O7} \rightarrow \sigma^*_{C1-O2}$ HOMO/LUMO interaction (cf. Scheme 3a), because even though the σ^*_{C1-O2} orbital is primarily localized on the more electropositive C1 atom, localization on the O2 atom is not trivial. NBO analysis of the HF/6-311+G(2d,p) wave function for conformer **3** indicates that the polarization coefficients for the σ^*_{C1-O2} orbital are 70% on C1 and 30% on O2 compared to 86% on Si and 14% on O7 for the σ^*_{O7-Si} orbital of conformer **2**. This means that the σ^*_{C1-O2} orbital lobes on the O2 atom are larger than the σ^*_{O7-Si} orbital lobes on the O7 atom, and hence the antibonding component of the $n_{O7} \rightarrow \sigma^*_{C1-O2}$ HOMO/LUMO interaction is larger than that of the $n_{O2} \rightarrow \sigma^*_{O7-Si}$ HOMO/LUMO interaction. Therefore, to overcome the destabilizing antibonding component of the $n_{O7} \rightarrow \sigma^*_{C1-O2}$ interaction between lobes of opposite sign and at the same time allow favorable bonding interaction between lobes of the same sign (cf. Scheme 3a), considerable C1−O2 and/or C6−O7 bond dissociation is necessary. In this case, there is greater dissociation of the weaker C1−O2 bond since the C6−O7 bond has double-bond character. Furthermore, significant C1−O2 bond dissociation results in features similar to that of a tight ion-pair intermediate comprising a methyl cation and a siloxycarbonyl anion (cf. Scheme 2b), where the n_{O2} and n_{O7} lone-pair orbitals

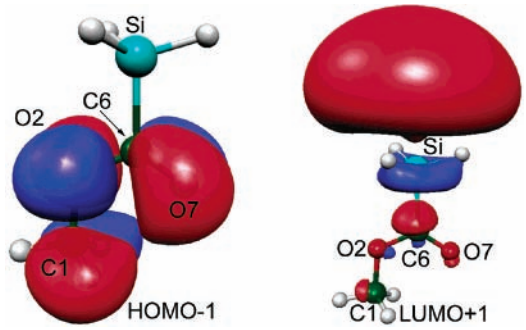

Figure 8. Relevant frontier molecular orbitals of *syn*-methyl silylformate, **5**, for decarbonylation involving intramolecular front-side nucleophilic attack by the methoxy oxygen O2 at silicon.

interact favorably with the "vacant cationic p orbital" on C1 in **TS$_{36}$** (cf. Scheme 3b).

Decarbonylation Involving Silyl Migration Followed by a Brook Rearrangement. Let us now turn to methoxy(siloxy)carbene decarbonylation involving initial 1,2-silyl migration to afford methyl silyl formate followed by a Brook ester rearrangement (cf. Scheme 4). As mentioned earlier, we have investigated the mechanism for 1,2-silyl migration in methoxy(siloxy)carbene.[13,14] However, we will briefly review some of the findings for completeness and then focus on decarbonylation via the Brook rearrangement.

In terms of frontier molecular orbital (FMO) theory,[20] 1,2-silyl migration is expected to occur via front-side nucleophilic attack by the carbene lone pair at silicon rather than an anion-like shift to the "vacant" carbene p orbital (cf. Scheme 6).[13,14] This is because the HOMO has carbene lone-pair n_{C6} orbital character while the LUMO is essentially the σ^*_{O7-Si} orbital (cf. Figure 3), and the geometries of conformers **1** and **3** are ideal for HOMO/LUMO interaction. We note that the former mechanism is *symmetry forbidden* (cf. Scheme 6a), while the latter mechanism is *symmetry allowed* (cf. Scheme 6b).

The optimized transition-state geometries **TS$_{14}$** and **TS$_{35}$** for 1,2-silyl migration in conformers **1** and **3** of methoxy(siloxy)carbene are shown in Figure 7. The corresponding products *anti*-methyl silylformate, **4**, and *syn*-methyl silylformate, **5**, as well as the transition state **TS$_{45}$** for isomerization between **4** and **5** are also shown in Figure 7. Relative to conformers **1** and **3** (cf. Figure 1), the ∠C6O7Si angles shrink considerably, while there is modest O7−Si bond lengthening and C6−O7 bond shortening in **TS$_{14}$** and **TS$_{35}$**. These geometric changes are accompanied by the appearance of a new C6−Si bond with low $\rho_b(r)$ and positive $\nabla^2\rho_b(r)$ in **TS$_{14}$** and **TS$_{35}$** (cf. Table 1), in concert with modest decreases and increases in $\rho_b(r)$ for the O7−Si and C6−O7 bonds, respectively. In addition, both **TS$_{14}$** and **TS$_{35}$** are planar, indicating that the silyl group migrates in the plane containing the carbene lone pair. These features are consistent with nucleophilic attack by the carbene C6 lone pair at silicon, along with O7−Si bond dissociation and C6−O7 double-bond formation.

We now turn to the decarbonylation of methyl silylformate via the Brook rearrangement. An examination of the HF/6-311+G(2d,p) frontier orbitals of methyl silylformate reveals that the relevant orbitals for front-side nucleophilic attack by the methoxy oxygen O2 at silicon are the HOMO-1 and the LUMO+1 rather than the HOMO and LUMO. Plots of the HOMO-1 and LUMO+1 for *syn*-methyl silylformate, **5**, are shown in Figure 8. As can be seen, the HOMO-1 has considerable n_{O2} character while the LUMO+1 has significant σ^*_{C6-Si} character. However, the calculated HF/6-311+G(2d,p) energy gap between these orbitals is 14.8 eV, which may be too large for favorable interaction and hence nucleophilic attack by the methoxy oxygen O2 at silicon. As a matter of fact, the HOMO-1/LUMO+1 gap is comparable to the HOMO/LUMO gaps of dimethoxycarbene[1] and methoxyphenoxycarbene[2] mentioned earlier, and these latter dioxycarbenes do not readily undergo intramolecular rearrangements. We also note that ester decarbonylation involving front-side nucleophilic attack by the methoxy oxygen at silicon is *symmetry forbidden*,[18−21] since the $n_{O2} \rightarrow \sigma^*_{C6-Si}$ HOMO/LUMO interaction contains a destabilizing antibonding component (cf. Scheme 6c).

The transition-state geometry **TS$_{56}$** for decarbonylation of *syn*-methyl silylformate, **5**, involving front-side nucleophilic attack by the methoxy oxygen O2 at silicon is shown in Figure 7. Relative to **5**, there is significant shrinkage of the ∠O2C6Si angle in **TS$_{56}$**, along with tremendous O2−C6 bond elongation and slight C6−Si bond lengthening and C6−O7 bond shortening. These geometric changes are accompanied by formation of an O2−Si bond with low $\rho_b(r)$ and positive $\nabla^2\rho_b(r)$, a dramatic decrease in $\rho_b(r)$ for the O2−C6 bond, while $\rho_b(r)$ decreases and increases modestly for the C6−Si and C6−O7 bonds, respectively (cf. Table 1). In addition, the methyl group rotates out of plane in **TS$_{56}$**. These features are in keeping with nucleophilic attack by methoxy oxygen O2 at silicon, in concert with tremendous O2−C6 bond dissociation, slight C6−Si bond dissociation, and modest C6−O7 triple-bond formation. The fact that O2−C6 bond dissociation is considerably greater than C6−Si bond dissociation in **TS$_{56}$** indicates that this *symmetry-forbidden* concerted reaction is *asynchronous*. Apparently, tremendous O2−C6 bond dissociation is necessary to overcome the sizable destabilizing antibonding component of the $n_{O2} \rightarrow \sigma^*_{C6-Si}$ HOMO/LUMO interaction (cf. Scheme 6c), because even though the σ^*_{C6-Si} orbital is primarily localized on Si, there is considerable localization on C6. In fact, NBO analysis of the HF/6-311+G(2d,p) wave function for ester **5** reveals that the polarization coefficients are 69 and 31% on Si and C6, respectively.

Energetics of Decarbonylation Pathways. We now examine the energetics of the pathways for methoxy(siloxy)carbene decarbonylation. From the relative ZPE-corrected electronic energies in Table 2 and Figure 2, it is apparent that decarbonylation involving front-side nucleophilic attack by the methoxy oxygen O2 at silicon in conformer **2** (via **TS$_{26}$**) is much more favorable than that involving front-side nucleophilic attack by the siloxy oxygen O7 at the methyl carbon C1 in conformer **3** (via **TS$_{36}$**). Decarbonylation involving initial 1,2-silyl migration followed by a Brook rearrangement also turns out to be unfavorable because, even though the initial 1,2-silyl migration in conformers **1** and **3** (via **TS$_{14}$** and **TS$_{35}$**) is quite facile, the Brook rearrangement of ester **5** (via **TS$_{56}$**) is unfavorable. We note that the computed barriers for the various reaction pathways above are in keeping with predictions made earlier on the basis of FMO theory. We also investigated the possibility of decarbonylation occurring via the intermediacy of a methoxy radical, carbon monoxide, and a silyl radical [$H_3CO^{\bullet}$ + CO + $^{\bullet}SiH_3$], as well as a methyl radical, carbon monoxide, and a silyloxy radical [$H_3C^{\bullet}$ + CO + $^{\bullet}OSiH_3$], similar to decarbonylation of diethoxycarbene[6] and methoxycarbene.[15] It is quite clear from the relative ZPE-corrected electronic energies in Table 2 and Figure 2 that decarbonylation via pathways involving these radicals is energetically unfavorable. Thus, it appears that the most viable pathway for methoxy(siloxy)carbene decarbonyla-

tion is that involving intramolecular front-side nucleophilic attack by the methoxy oxygen O2 at silicon in conformer **2** via $\mathbf{TS_{26}}$.

Finally, to further connect the results from our investigation of methoxy(siloxy)carbene with the experimental results on methoxytriphenylsiloxycarbene, we performed calculations for the latter species with a lower-level model chemistry (B3LYP/6-311+G(2d,p)//B3LYP/6-31G*) because of the system size. According to our calculations, the transition state for decarbonylation of methoxytriphenylsiloxycarbene via the concerted pathway involving intramolecular front-side nucleophilic attack by the methoxy oxygen at silicon lies 25.6 kcal/mol above the (lowest-energy) *trans-trans* conformer of methoxytriphenylsiloxycarbene. On the other hand, the intermediacy of a methoxy radical, carbon monoxide, and a triphenylsilyl radical [$H_3CO^{\bullet}$+CO+$^{\bullet}SiPh_3$] lies 67.7 kcal/mol above *trans-trans*-methoxytriphenylsiloxycarbene, while that of a methyl radical, carbon monoxide, and a triphenylsilyloxy radical [$H_3C^{\bullet}$ + CO + $^{\bullet}OSiPh_3$] lies 49.3 kcal/mol above *trans-trans*-methoxytriphenylsiloxycarbene.[58] Compared to methoxy(siloxy)carbene (cf. Table 2 and Figure 3), the presence of phenyl groups on the silyl moiety of methoxytriphenylsiloxycarbene slightly raises the barrier for decarbonylation via the concerted pathway, while it appears to have no pronounced effect on the stabilities of the silyl and silyloxy radicals. Hence, the most energetically viable pathway for decarbonylation of methoxytriphenylsiloxycarbene is indeed that involving intramolecular front-side nucleophilic attack by the methoxy oxygen at silicon.

Conclusion

The decarbonylation of methoxy(siloxy)carbene was investigated by means of ab initio molecular orbital theory and hybrid DFT calculations, combined with the quantum theory of atoms in molecules (AIM). Pathways involving intramolecular front-side nucleophilic attack by the methoxy oxygen at silicon and by the siloxy oxygen at the methyl carbon were investigated. The pathway involving front-side attack by the methoxy oxygen at silicon was found to be concerted and synchronous. In contrast, even though the pathway involving front-side nucleophilic attack by the siloxy oxygen at the methyl carbon was found to be concerted, it is asynchronous, with a transition state resembling that of a tight ion-pair intermediate comprising a methyl cation and a siloxycarbonyl anion. A decarbonylation pathway involving initial silyl migration followed by a Brook ester rearrangement, and pathways involving the intermediacy of radicals were also examined. The pathway involving initial 1,2-silyl migration followed by a Brook rearrangement was found to be unfavorable because of the thermodynamic stability of methyl silylformate. Fragmentation−recombination mechanisms involving the intermediacy of radicals [$H_3CO^{\bullet}$ + CO + $^{\bullet}SiH_3$], and [$H_3C^{\bullet}$ + CO + $^{\bullet}OSiH_3$] are also energetically unfavorable. Thus, it appears that the most viable pathway for decarbonylation of methoxy(siloxy)carbene is that involving intramolecular front-side nucleophilic attack by the methoxy oxygen at silicon.

Acknowledgment. This work was funded by research grants from the Natural Science and Engineering Research Council of Canada and the Fonds pour la Formation des Chercheurs et l'Aide à la Recherche (FCAR-Québec). Calculations were performed at the Centre for Research in Molecular Modeling, which was established with the financial support of the Concordia University Faculty of Arts & Science, the Ministère de l'Éducation du Québec, and the Canada Foundation for Innovation. G.H.P. holds a Concordia University Research Chair. The authors thank Dr. Heidi Muchall for helpful discussion and anonymous reviewers for useful suggestions.

Supporting Information Available: Topological properties of the electronic density at pertinent BCPs based on AIM analysis of HF/6-311+G(2d,p) and MP2/6-311+G(2d,p) wave functions are provided. Also, Cartesian coordinates and absolute electronic energies are supplied for optimized geometries, and imaginary frequencies are given for all transition states. The computed HF/6-311+G(2d,p) ZPE-corrected electronic energies are also provided. This information is available on the web at http://pubs.acs.org.

References and Notes

(1) Moss, R. A.; Wlostowski, M.; Shen, S.; Krogh-Jespersen, K.; Matro, A. *J. Am. Chem. Soc.* **1988**, *110*, 4443.
(2) Moss, R. A.; Wlostowski, M.; Terpinski, J.; Krogh-Jespersen, K. *J. Am. Chem. Soc.* **1987**, *109*, 3811.
(3) Lu, X.; Warkentin, J. *Can. J. Chem.* **2001**, *79*, 364.
(4) Lu, X.; Reid, D. L.; Warkentin, J. *Can. J. Chem.* **2001**, *79*, 319.
(5) El-Saidi, M.; Kassam, K.; Pole, D. L.; Tadey, T.; Warkentin, J. *J. Am. Chem. Soc.* **1992**, *114*, 8751.
(6) Crawford, R. J.; Raap, R. *Proc. Chem. Soc.* **1963**, 370.
(7) Venneri, P. C.; Warkentin, J. *J. Am. Chem. Soc.* **1998**, *120*, 11182.
(8) Reid, D. L.; Hernandez-Trujillo, J.; Warkentin, J. *J. Phys. Chem. A* **2000**, *104*, 3398.
(9) Reid, D. L.; Warkentin, J. *J. Chem. Soc., Perkin Trans. 2* **2000**, 1980.
(10) Merkley, N.; El-Saidi, M.; Warkentin, J. *Can. J. Chem.* **2000**, *78*, 356.
(11) Merkley, N.; Warkentin, J. *Can. J. Chem.* **2000**, *78*, 942.
(12) Pezacki, J. P.; Loncke, P. G.; Ross, J. P.; Warkentin, J.; Gadosy, T. A. *Org. Lett.* **2000**, *2*, 2733.
(13) Loncke, P. G.; Gadosy, T. A.; Peslherbe, G. H. *Can. J. Chem.* **2002**, *80*, 302.
(14) Loncke, P. G.; Gadosy, T. A.; Peslherbe, G. H. *Arkivok* **2001**, *2*, 179.
(15) McDonald, R. M.; Krueger, R. A. *J. Org. Chem.* **1966**, *31*, 488.
(16) Schreiner, P. R.; Schleyer, P.; Hill, R. K. *J. Org. Chem.* **1993**, *58*, 2822.
(17) Schreiner, P. R.; Schleyer, P.; Hill, R. K. *J. Org. Chem.* **1994**, *59*, 1849.
(18) Hoffmann, R.; Woodward, R. B. *Acc. Chem. Res.* **1968**, *1*, 17.
(19) Woodward, R. B.; Hoffmann, R. *Angew. Chem., Int. Ed. Engl.* **1969**, *8*, 781.
(20) Fleming, I. *Frontier Orbitals and Organic Chemical Reactions*; John Wiley & Sons: Ltd.: Chichester, 1976.
(21) Fukui, K. *Science* **1982**, *218*, 747.
(22) We note that carbonyl anions, sometimes referred to as acyl or formyl anions, do exist (cf. Graul, S.; Squires, R. R. *J. Am. Chem. Soc.* **1988**, *110*, 607; Chandrasekhar, J.; Andrade, J. G.; Schleyer, P. v. R. *J. Am. Chem. Soc.* **1981**, *103*, 5612 and references therein).
(23) Moss, R. A.; Zheng, F.; Johnson, L. A.; Sauers, R. R. *J. Phys. Org. Chem.* **2001**, *14*, 400.
(24) Yan, S.; Sauers, R. R.; Moss, R. A. *Org. Lett.* **1999**, *1*, 1603.
(25) Moss, R. A. *Acc. Chem. Res.* **1999**, *32*, 969.
(26) Moss, R. A.; Johnson, L. A.; Merrer, D. C.; Lee, G. E., Jr. *J. Am. Chem. Soc.* **1999**, *121*, 5940.
(27) Moss, R. A.; Ge, C. *J. Am. Chem. Soc.* **1996**, *118*, 9792.
(28) Moss, R. A.; Balcerzak, P. *J. Am. Chem. Soc.* **1992**, *114*, 9386.
(29) Moss, R. A.; Zdrojewski, T. *Tetrahedron Lett.* **1991**, *32*, 5667.
(30) Moss, R. A.; Kim, H.-R. *Tetrahedron Lett.* **1990**, *31*, 4715.
(31) Moss, R. A.; Ho, G. J.; Wilk, B. K. *Tetrahedron Lett.* **1989**, *30*, 2473.
(32) Moss, R. A.; Wilk, B. K.; Hadel, L. M. *Tetrahedron Lett.* **1987**, *28*, 1969.
(33) Brook, A. G. *J. Am. Chem. Soc.* **1955**, *77*, 4827.
(34) Brook, A. G. *Acc. Chem. Res.* **1974**, *7*, 77.
(35) Hehre, W. J.; Radom, L.; Schleyer, P. v. R.; Pople, J. A. *Ab Initio Molecular Orbital Theory*; John Wiley & Sons: New York, 1986.
(36) Jensen, F. *Introduction to Computational Chemistry*; John Wiley & Sons Ltd.: Baffins Lane, 1999.
(37) Becke, A. D. *J. Chem. Phys.* **1993**, *98*, 5648.
(38) Frisch, M. J.; Trucks, G. W.; Schlegel, H. B.; Scuseria, G. E.; Robb, M. A.; Cheeseman, J. R.; Zakrzewski, V. G.; Montgomery, J. A., Jr.; Stratmann, R. E.; Burant, J. C.; Dapprich, S.; Millam, J. M.; Daniels, A. D.; Kudin, K. N.; Strain, M. C.; Farkas, O.; Tomasi, J.; Barone, V.; Cossi, M.; Cammi, R.; Mennucci, B.; Pomelli, C.; Adamo, C.; Clifford, S.;

Ochterski, J.; Petersson, G. A.; Ayala, P. Y.; Cui, Q.; Morokuma, K.; Malick, D. K.; Rabuck, A. D.; Raghavachari, K.; Foresman, J. B.; Cioslowski, J.; Ortiz, J. V.; Stefanov, B. B.; Liu, G.; Liashenko, A.; Piskorz, P.; Komaromi, I.; Gomperts, R.; Martin, R. L.; Fox, D. J.; Keith, T.; Al-Laham, M. A.; Peng, C. Y.; Nanayakkara, A.; Gonzalez, C.; Challacombe, M.; Gill, P. M. W.; Johnson, B. G.; Chen, W.; Wong, M. W.; Andres, J. L.; Head-Gordon, M.; Replogle, E. S.; Pople, J. A. *Gaussian 98*, revision A.11.4; Gaussian, Inc.: Pittsburgh, PA, 1998.

(39) Schlegel, H. B. *J. Comput. Chem.* **1982**, *3*, 214.

(40) Bannerjee, A.; Adams, N.; Simons, J.; Shepard, R. *J. Phys. Chem.* **1985**, *89*, 52.

(41) Simons, J.; Jorgensen, P.; Taylor, H.; Ozment, J. *J. Phys. Chem.* **1983**, *87*, 2745.

(42) Cerjan, C. J.; Miller, W. H. *J. Chem. Phys.* **1981**, *75*, 2800.

(43) Ochterski, J. W. *Thermochemistry in Gaussian*; Gaussian Inc.: Pittsburgh, PA, 2000.

(44) Bader, R. F. W. *Atoms in Molecules. A Quantum Theory*; Clarendon Press: Oxford, 1990.

(45) The AIMPAC suite of programs is available from Professor R. F. W. Bader, McMaster University, Canada, and from the AIMPAC website (www.chemistry.mcmaster.ca/aimpac).

(46) Biegler-Konig, F. W.; Bader, R. F. W.; Tang, T. *J. Comput. Chem.* **1982**, *3*, 317.

(47) Reed, A. E.; Curtiss, L. A.; Weinhold, F. *Chem. Rev.* **1988**, *88*, 899.

(48) Glendening, E. D.; Reed, A. E.; Carpenter, J. E.; Weinhold, F. *NBO 3.0 Program Manual*; Theoretical Chemistry Institute and Department of Chemistry, University of Wisconsin: Madison, Wisconsin.

(49) The Laplacian of the electronic density allows identification of regions of local charge concentration ($\nabla^2\rho(r) < 0$) and local charge depletion ($\nabla^2\rho(r) > 0$) in the topology of the electronic density (cf. ref 44).

(50) VSCC refers to the region of charge concentration corresponding to the outermost quantum shell of an atom where the Laplacian of the electronic density is negative (cf. ref 44).

(51) A BCP is the point of minimum electronic density $\rho(r)$ along a bond or bond path (cf. ref 44).

(52) The bond ellipticity ϵ is a measure of the extent to which charge preferentially accumulates in a given plane along a bond or *bond path*. A value of zero reflects the cylindrical symmetry usually associated with single or triple bonds and a value larger than zero is indicative of the elliptical symmetry often associated with double bonds (cf. ref 44).

(53) Moss, R. A.; Xue, S.; Liu, W.; Krogh-Jespersen, K. *J. Am. Chem. Soc.* **1996**, *118*, 12588.

(54) A low $\rho_b(r)$ and positive $\nabla^2\rho_b(r)$ are characteristic of a weak bond, while a large $\rho_b(r)$ and negative $\nabla^2\rho_b(r)$ are characteristics of a strong covalent bond (cf. ref 44).

(55) Sommer, L. H.; Fujimoto, H. *J. Am. Chem. Soc.* **1968**, *90*, 982.

(56) Sommer, L. H. *Stereochemistry, Mechanism and Silicon: An Introduction to the Dynamic Stereochemistry and Reaction Mechanisms of Silicon Centers*; McGraw-Hill Book Company: New York, 1965.

(57) Sommer, L. H.; McLick, J.; Golino, C. M. *J. Am. Chem. Soc.* **1972**, *94*, 669.

(58) The energies of the triphenylsilyl and triphenylsilyloxy radicals were obtained from ROB3LYP/6-311+G(2d, p) calculations based on ROB3LYP/6-31G* optimized geometries.